Supporting Information

Leveraging Self-Passivation of Quantum Dots via Nitrogen-Doping for Multifunctional Biopolymer Nanocomposites

Anthony V. Tuccitto [a,b], Rafaela Aguiar [a], Nello D. Sansone [a], Yalda Chehrehsaz [a], Boran Kumral [b], Peter Serles [b], Tobin Filleter [b], Chul B. Park [b], Patrick C. Lee [a] *

*Corresponding Authors: patricklee@mie.utoronto.ca

[a] Multifunctional Composites Manufacturing Laboratory (MCML), Department of Mechanical and Industrial Engineering, University of Toronto, 5 King's College Road, Toronto, M5S 3G8, Canada.

[b] Department of Mechanical and Industrial Engineering, University of Toronto, 5 King's College Road, Toronto, M5S 3G8, Canada.

Rationale for QD precursor composition

While there have been previous accounts of QDs derived from CA:Urea precursor ratios up to 1:100,[1] there are limitations in the practical applicability of using such QDs in high transparency nanocomposites, particularly with regards to the light absorption in the visible light region.

Specifically, increasing the urea precursor content not only imparts a greater degree of N- in the carbon framework, but also increases the proportion of graphitic-N in the QDs. From our UV-Visible spectroscopy measurements in **Fig. 4**, this may reduce the light excitation energy barrier (i.e., increases absorption wavelength). If further urea content was used in QD synthesis, we anticipate more intense light absorption in the UV- and blue-light regions, with more pronounced absorption of longer visible light wavelengths owing to further delocalization of excited graphitic-N electrons. This consequently leads to more pronounced light absorption in the visible region, which would detriment greatly the visible light transmittance (VLT) of the nanocomposites. This is evident in the UV-visible spectroscopy data shown in **Fig. 4A** illustrating that even a 1:3 ratio of CA:urea imparts a very large absorption band in the visible region, which contributes to the reduced VLT of the 0.25 wt.% NGO-QD2 nanocomposite film. Nevertheless, we found that at a concentration of 0.25 wt.%, the CA:urea ratio that permits the greatest UV absorption and pronounced blue-light absorption is 1:3 CA:Urea, which still provides transparent nanocomposites (> 70% VLT).

Moreover, it should be noted that there must be a balance between the CA:urea precursor ratio and the QD concentration in PLLA to fabricate nanocomposites with sufficiently high VLT. While varying the CA:urea precursor ratio of QDs can result in more pronounced UV- and visible light absorption owing to a different density of graphitic-N groups, it is plausible that a high VLT for such nanocomposites could be attained via changes in the QD content.

Detailed solution blending procedure

Owing to the dissimilar compositions of the synthesized GO-QD derivatives, it is challenging to disperse all particles well using a single solvent. As such, we developed an emulsion-based approach incorporating solvents with varying degrees of polarity to promote dispersion of all GO-QD derivatives in the PLLA matrix. First, 150 mL of DCM was added to a 250 mL glass jar under vigorous stirring (900 rpm). Then, 37.5 mL of Acetone, 8.8 mL of ethanol, and 3.99 g of distilled water were sequentially added to the jar. This mixture forms an unstable water-in-oil emulsion that phase-separates upon cessation of agitation. Then, 14.9625 g (15.000 g for the case of neat PLLA

samples) of PLLA was added to the emulsion, which was dissolved over 2 h under ambient conditions. Upon dissolution of PLLA, the emulsion stability was increased (stable for ~ 30 min). After PLLA dissolution, 0.0375 g of each GO-QD derivative was added separately into their respective PLLA-emulsions. These mixtures were stirred vigorously (900 rpm) for 60 min. Each solution was subject to ultrasonication using a point sonicator probe (QSONICA Q500, Power: 500 W). Solutions were separated into two equal aliquots by volume in 125 mL beakers, and each sonicated at 70 % power, on cycles of 4 min duration (pulse 10 s on, 10 s off), in a water bath. Solutions were then cooled for 1 min after this sonication process. Each respective solution was sonicated another time at 70 % power with cycles of 4 min duration (pulse 10 s on, 10 s off). Sonicated blend solutions were cast into large aluminum trays (30 cm × 45 cm), and the solvent was allowed to dry for 2 h in a fumehood. Cast films were then dried at 40 °C under vacuum for 3 days, to ensure solvent removal. The resulting blends contained 0.25 wt.% of each GO-QD derivative in the PLLA matrix.

Fourier transform infrared spectroscopy

Fourier Transform Infrared Spectroscopy (FTIR) was used to compare the functional groups present on each GO-QD derivative, as well as to compare their surface functionalities with the CA and urea precursors. A Thermo Scientific iS50 ATR FTIR was used for analysis in the range of 4000 cm^{-1} to 350 cm^{-1}, with a resolution of 4 cm^{-1}, and 128 scans. Spectroscopic measurements were conducted on at least 3 batches of each GO-QD derivative to validate repeatability, with representative spectra reported. FTIR was also used to characterize the intermolecular interactions present in QD-nanocomposites as hydrogen bonding or covalent bonding interactions. Nanocomposites were compression molded into films of 1.90 mm in thickness, and were analyzed using the same experimental parameters as were described above.

X-Ray photon spectroscopy and Zeta potential measurements

X-ray photon spectroscopy (XPS) was conducted on each GO-QD derivative to quantify the surface functional groups of the GO-QD derivatives, using a ThermoFisher Scientific K-Alpha system. The zeta potential of the GO-QDs prepared were analyzed using a Brookhaven Instruments Corporation ZetaPlus Zeta Potential Analyzer using DI water (pH = 7) for all GO-QDs, and a red laser light source with a wavelength of 660 nm, similar to related work.[2]

Atomic force microscopy

Atomic force microscopy (AFM) was employed to characterize the size of the synthesized GO-QD derivatives. Each GO-QD derivative was ultrasonically dispersed in DI water at a concentration of 0.1 wt.%, filtered through a 20 nm filter to remove large agglomerates formed during lyophilization, and were drop cast on a silicon wafer. Regions containing GO-QDs on a silicon wafer were imaged using an AFM (Asylum Research Cypher) in tapping mode with a silicon AFM probe on an Al-coated silicon cantilever (NANOSENSORS PPP-NCHR-20). Scans were performed over 1×1, 1.5×1.5 and 2×2 μm areas at 256×256 pixels and 0.5 Hz. AFM data was evaluated using Gwyddion topography processing software, with data plotted using OriginPro.

Calorimetric analysis

The non-isothermal calorimetric behavior of neat PLLA and nanocomposites containing the synthesized GO-QD derivatives were studied by differential scanning calorimetry (DSC), using a TA instruments DSC 250. First, samples weighing between 5 – 10 mg were sealed in aluminum hermetic pans, and analyzed under nitrogen gas. Each sample was heated from 20 to 180 °C at a rate of 10 °C/min. The samples were then heated at 180 °C for 3 min to erase the previous thermal history. Samples were then cooled at different cooling rates of 50, 20, 10, 5, and 2 °C/min to 20 °C. The samples were equilibrated at 20 °C for 2 min to account for thermal lag and were subsequently heated at a rate of 10 °C/min to 180 °C to analyze the crystal structures formed during each cooling profile.

The homocrystal (HC) degree of crystallinity $\chi_{c(HC)}$ of PLLA was calculated for each heating cycle using the following equation as was used in previous work:[3]

$$\chi_{c(HC)}(\%) = \frac{\Delta H_{m,HC} - \Delta H_{cc}}{\Delta H_{m,HC}^{0} \cdot w_{PLLA}} \times 100\%$$

where, the $\Delta H_{m,HC}$ is the enthalpy of fusion of PLLA HCs, ΔH_{cc} is the enthalpy of cold crystallization which accounts for the fraction of crystals nucleated during calorimetric heating ramps, w_{PLLA} is the weight fraction of PLLA, and $\Delta H_{m,HC}^{0}$ is the theoretical enthalpy of fusion of PLLA that is 100 % crystalline (93.6 J/g).[4]

Polarized optical microscopy

A polarized optical microscope (POM, Olympus BX53M) coupled with a Linkam CSS 450 stage possessing heating/cooling capabilities was used to study the isothermal crystallization kinetics of the neat PLLA and QD-containing nanocomposites. First, thin films of ~ 20 μm in thickness were melted at 180 °C for 3 min, followed by rapid cooling at 35 °C/min to an isothermal temperature of 130 °C. The melt was held at this temperature for 30 min, and micrographs illustrating the evolution of crystals from the amorphous melt were obtained every 1 s. Images were obtained using a 50 × magnification objective lens, coupled with an Olympus U-TP530 wave plate.

Optical transparency and light absorption characterization

Rectangular films of neat PLLA and its QD-reinforced nanocomposites with thickness of 150 μm were analyzed using a dual beam Lambda 365 UV/Vis Spectrometer (PerkinElmer, USA), to quantify film UV- and visible-light transparency. Data acquisition was conducted at room temperature over wavelengths ranging from 200 – 1000 nm. Three replicate measurements were obtained for each sample type, with reported spectra being an average of the 3 replicate spectral measurements. The visible light transmittance (VLT) of PLLA-based films was calculated similar to previous work,[5] relative to the CIE D65 illuminant,[6] while light blocking ability was calculated for distinct spectral regions (Blue: 400 – 500 nm, UVA: 320 – 400 nm, UVB: 290 – 320 nm, UVC: 260 – 290 nm) as the area under the UV-visible spectrum relative to 100 % spectral transmittance.[7] Images illustrating the fluorescence emission of QD-nanocomposites were obtained by sealing compression molded circular disks (25 mm diameter, 1 mm thickness), or thin films (150 μm thickness) in a closed box, followed by illumination with UV-LED (365 or 395 nm, Police Security & Élite) approximately 10 cm above each respective film.

Reflectance wavelength measurements of the molded films were performed using a Nix Spectro 2 Spectrophotometer (Nix Sensor Ltd, Canada) in the range of 400 – 700 nm. Each PLA film was individually sandwiched between the spectrophotometer and a white background film for a consistent background, with reflectance measurements obtained hereafter. All spectrophotometer measurements were conducted at room temperature.

Rheological characterization

Shear oscillatory rheological measurements were conducted using an ARES G2 rheometer with parallel plate fixtures. The plate diameter was 25 mm, with a gap of 1 mm used for rheological characterization. Strain sweeps were conducted to identify the linear viscoelastic region of neat PLLA and its blends with GO-QD derivatives. A fixed strain of 5 % (within the linear viscoelastic region) was selected for frequency sweeps ranging from 500 to 0.1 rad/s. All experiments were conducted at 180 °C with data reported as an average of duplicate measurements.

Tensile tests

Injection molded specimens were prepared using a piston-based microinjection system (Xplore IM 5.5), to identify the effects of the GO-QD derivatives on PLLA's tensile performance. First, 2.5 g batches of vacuum-dried blends produced via solution blending were melted at 180 °C for 3 min in the machine barrel, and then molded into an ASTM Type V dogbone mold at 65 °C with an injection pressure of 1.6 MPa for 30 s to facilitate cooling. Under these molding conditions, crystallization is largely inhibited, and the intrinsic effect of the filler particles can be discerned.

Injection molded tensile dogbones were subject to tensile tests at room temperature using an Instron Universal Testing System with a crosshead speed of 5 mm/min. All samples were sealed in air-tight containers and aged for 48 hr under ambient conditions prior to tensile tests. Tensile property values are reported as average values with 4 specimen replicates.

Scanning electron microscopy

An FEI Quanta FEG 250 Scanning electron microscope was used to analyze the morphology of each tensile test specimen's fracture surface. Nanocomposite fracture surface specimens were mounted onto SEM stubs using carbon tape, coated using a carbon evaporator (EMITECH K950X), and analyzed under an acceleration voltage of 5.00 kV.

Statistical analysis

Data in figures are represented by mean and standard deviations (SD)s, with statistical analyses performed using GraphPad Prism software. One-Way ANOVA (Analysis of Variance) was applied to the VLT and light-blocking data (**Fig. 4B**, **Fig. S1**), as well as tensile data (**Fig. 7**), and was paired with Dunnett's multiple comparisons test. Labels ns, *, **, ***, **** represent significance levels of $p > 0.05$, $p < 0.05$, $p < 0.01$, $p < 0.001$, and $p < 0.0001$, respectively. All statistical comparisons were made between the neat PLLA control and a given QD-containing nanocomposite. Statistical data obtained from these tests can be found in **Table S5**.

Supporting results and discussion

Table S1. Elemental identification and quantification obtained from full-spectrum XPS analysis.

Sample Name	Atomic Percentage (%)				
	Carbon	**Nitrogen**	**Oxygen**	**Silicon**	**Sodium**
GO-QD	47.31	0.11	35.16	0	17.42
NGO-QD1	60.90	7.77	25.43	1.25	4.65
NGO-QD2	63.02	12.14	24.07	0.71	0.06

The UV-visible transmittance spectra of neat PLLA and nanocomposite films containing 0.1 and 0.25 wt.% NGO-QD2 are illustrated in **Figure S1D**, with corresponding light blocking ability in **Figure S1E**. Here, similar absorption bands to the 0.25 wt.% NGO-QD2 film are observed for the 0.1 wt.% NGO-QD2 film, but with lower intensities than for the 0.25 wt.% NGO-QD2 film, as expected. With 0.1 wt.% NGO-QD2, films exhibit blue, UVA, UVB, and UVC light blocking abilities of 39.7 ± 1.5, 44.8 ± 1.8, 50.8 ± 1.5 and 69.9 ± 2.3%, with a VLT of 79.1 ± 0.8%.

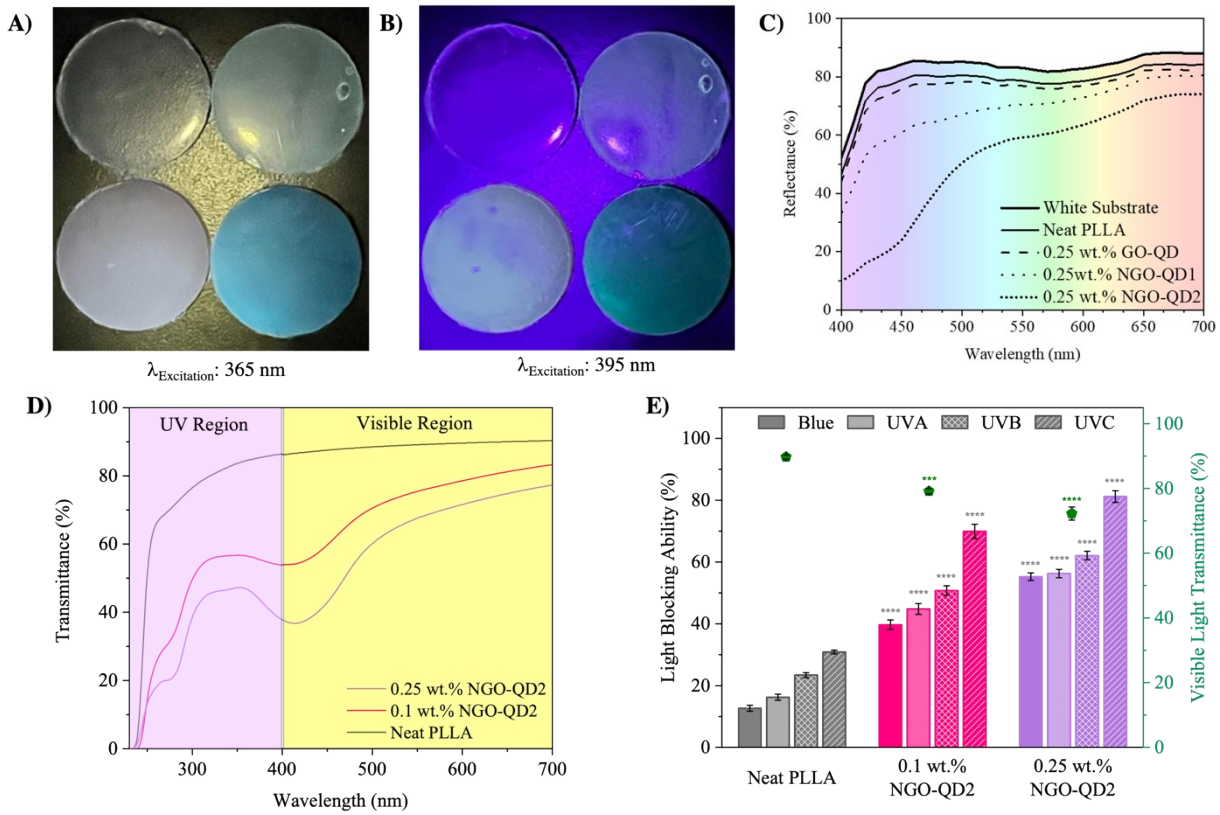

Fig. S1. A) Image of PLLA and nanocomposites under 365 nm blacklight excitation, and **B)** image of PLLA and nanocomposites under 395 nm blacklight excitation, illustrating their fluorescence behavior, **C)** visible light reflectance of neat PLLA and QD-nanocomposite films. Films were sandwiched between a white reflective film and the spectrophotometer. Reflectance in the blue-light region is minimized in the presence of N-containing QDs, **D)** UV-Visible transmittance spectra of PLLA and nanocomposite films averaged over 3 replicate measurements, **E)** visible-light transmittance and light blocking ability of PLLA and nanocomposite films. The thickness of films used in UV-visible spectroscopy measurements is fixed at 150 μm. Blue-light, UVA, UVB, and UVC correspond to wavelength regions of 400 – 500, 320 – 400, 290 – 320, and 260 – 290 nm, respectively. Statistical analysis was conducted for light-blocking ability measurements of QD-containing nanocomposites relative to the control, in each respective wavelength region.

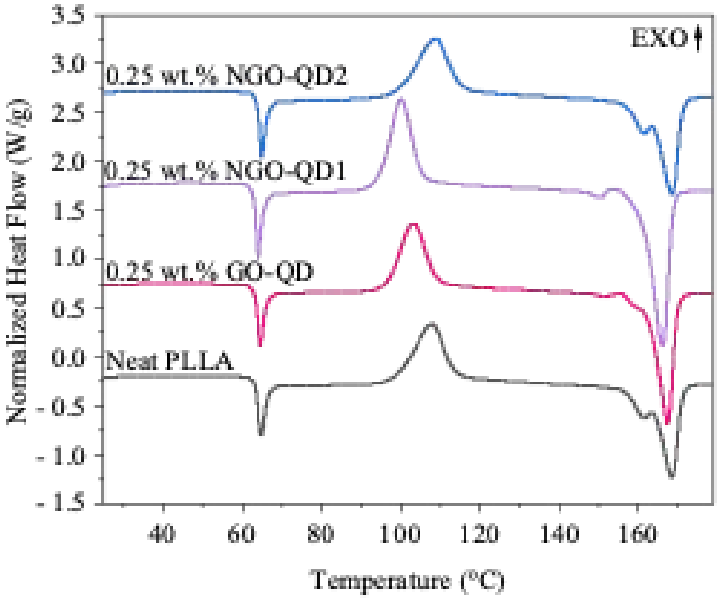

Fig. S2. DSC 1st heating curves corresponding to neat PLLA and QD-nanocomposite films, obtained using a heating rate of 10 °C/min. The presented calorimetric data are shifted by an arbitrary value for each respective specimen.

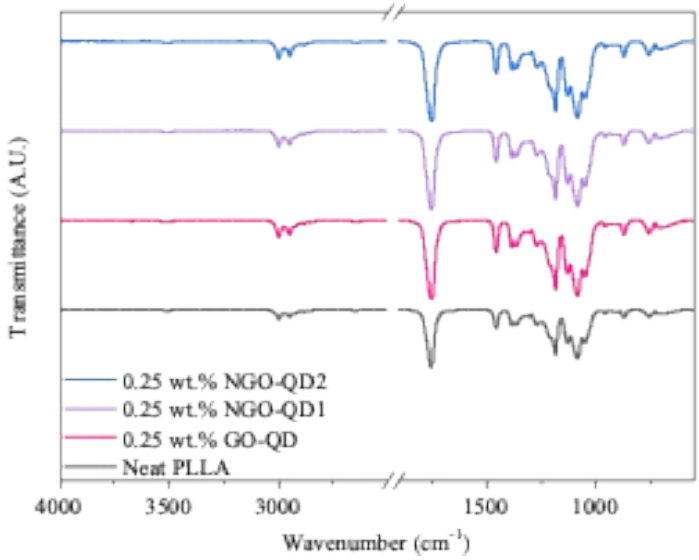

Fig. S3. FTIR Spectra of neat PLLA and QD-nanocomposites. The similar spectra amongst samples, and lack of broad O–H stretching band suggest that H-bonding interactions do not greatly affect the UV-visible spectral observations.

Table S2. Thermal phase transition data for neat PLLA and QD-nanocomposites obtained from non-isothermal calorimetric cooling treatments at various cooling rates.

Thermal Parameters	Neat PLLA	0.25 wt.% GO-QD	0.25 wt.% NGO-QD1	0.25 wt.% NGO-QD2
Applied Cooling Rate: 20 °C·min^{-1}				
$T_{c,peak}$ (°C)	88.7	88.4	88.1	85.8
$\Delta H_{c,peak}$ (J/g)	0.67	2.90	2.35	0.96
Applied Cooling Rate: 10 °C·min^{-1}				
$T_{c,peak}$ (°C)	93.6	89.3	92.4	90.1
$\Delta H_{c,peak}$ (J/g)	2.47	24.8	27.2	11.6
Applied Cooling Rate: 5 °C·min^{-1}				
$T_{c,peak}$ (°C)	98.3	108.0	110.4	96.5
$\Delta H_{c,peak}$ (J/g)	10.2	52.1	53.3	45.7
Applied Cooling Rate: 2 °C·min^{-1}				
$T_{c,peak}$ (°C)	114.4	114.9	117.0	119.5
$\Delta H_{c,peak}$ (J/g)	35.0	53.0	56.3	55.0

Table S3. Thermal phase transition data for neat PLLA and QD-nanocomposites obtained from non-isothermal calorimetric heat treatments after cooling at various cooling rates.

Thermal Parameters	Neat PLLA	0.25 wt.% GO-QD	0.25 wt.% NGO-QD1	0.25 wt.% NGO-QD2
After Applied Cooling Rate: 20 °C·min^{-1}				
T_g (°C)	59.7	48.7	49.4	51.0
T_{cc} (°C)	115.4	100.4	97.4	103.8
ΔH_{cc} (J/g)	26.0	40.7	41.7	38.1
$T_{m,peak}$ (°C)	167.3	162.8	164.0	166.9
$\Delta H_{m,peak}$ (J/g)	29.0	47.6	49.9	42.8
After Applied Cooling Rate: 10 °C·min^{-1}				
T_g (°C)	59.6	45.0	47.2	49.6
T_{cc} (°C)	115.0	93.6	93.2	97.5
ΔH_{cc} (J/g)	26.1	20.5	19.1	27.8
$T_{m,peak}$ (°C)	168.4	159.3	161.4	165.4
$\Delta H_{m,peak}$ (J/g)	32.5	49.3	50.4	43.9
After Applied Cooling Rate: 5 °C·min^{-1}				
T_g (°C)	59.8	-	-	-
T_{cc} (°C)	115.8	-	-	-
ΔH_{cc} (J/g)	22.9	-	-	-
$T_{m,peak}$ (°C)	168.9	157.0	159.2	165.1
$\Delta H_{m,peak}$ (J/g)	34.0	52.3	54.5	47.4
After Applied Cooling Rate: 2 °C·min^{-1}				
T_g (°C)	61.1	-	-	-
T_{cc} (°C)	120.7	-	-	-
ΔH_{cc} (J/g)	3.92	-	-	-
$T_{m,peak}$ (°C)	169.4	155.1	156.7	159.0

$\Delta H_{m,peak}$ (J/g)	39.7	53.2	56.6	57.6

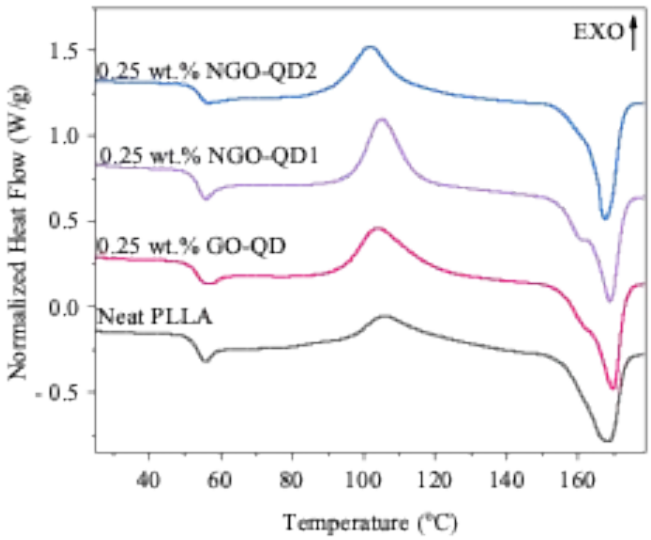

Fig. S4. DSC 1st heating curve of tensile test specimens heated at a rate of 10 °C/min. The degree of crystallinity of the neat PLLA and QD-nanocomposites are low (< 10 %). The presented calorimetric data are shifted by an arbitrary value for each respective specimen.

The rigid amorphous fraction (RAF) of tensile specimens was estimated by calorimetric analysis, similar to previous work.[8] With respect to the three-phase model of polymer phase behaviour, the RAF can be estimated as the polymer fraction that is neither crystallized, nor has true amorphous mobility (denoted by χ_{MAF}).

$$\chi_{RAF} = 100 - \chi_{C(HC)} - \chi_{MAF} \tag{S1}$$

Here, χ_{MAF} is estimated by the following relationship:

$$\chi_{MAF} = \frac{\Delta c_p}{\Delta c_p^a} \times 100\% \tag{S2}$$

where Δc_p is the change in heat capacity through T_g of the as-molded tensile specimen, while Δc_p^a is the change in heat capacity after quenching from the melt-state at 50 °C/min, to suppress crystal growth.

Table S4. Thermal properties of the neat PLLA and QD-nanocomposites. Peak temperatures are reported for each phase change. Degree of crystallinity is calculated assuming 93.6 J/g as the enthalpy of fusion for 100 % crystalline PLA.

Sample Name	T_g (°C)	Δc_p ($J \cdot g^{-1} \cdot °C^{-1}$)	Δc_p[a] ($J \cdot g^{-1} \cdot °C^{-1}$)	T_{cc} (°C)	ΔH_{cc} ($J \cdot g^{-1}$)	$T_{m,HC}$	$\Delta H_{m,HC}$ ($J \cdot g^{-1}$)	$\chi_{c,HC}$ (%)	χ_{MAF} (%)	χ_{RAF} (%)
Neat PLLA	52.3	0.498	0.534	106.6	29.4	168.6	33.7	4.6	93.2	2.2
0.25 wt.% GO-QD	52.2	0.492	0.523	104.5	30.0	169.8	35.4	5.5	94.1	0.4
0.25 wt.% NGO-QD1	52.4	0.470	0.508	105.3	30.0	169.1	36.0	6.4	92.5	1.1
0.25 wt.% NGO-QD2	53.2	0.495	0.529	102.2	30.3	167.8	34.8	4.8	93.6	1.6

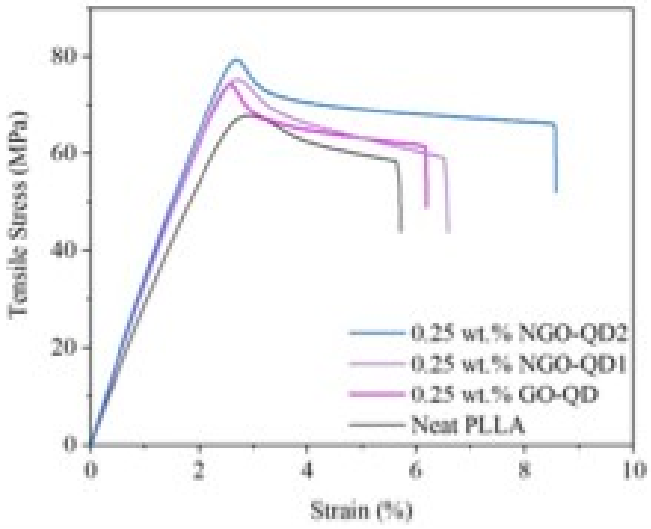

Fig. S5. Select stress-strain curves illustrating the tensile behavior of neat PLLA and QD-nanocomposites, obtained under a strain rate of 5 mm/min.

Table S5. Statistical analysis conducted using GraphPad Prism including One-way ANOVA and Dunnett's Multiple Comparison Test.

			One Way ANOVA		Dunnett's Multiple Comparisons	
Figure	**Data Description**	**Group Size (n)**	**F (Dfn,DFd)**	**ANOVA P Value**	**Sample Name**	**Adjusted p Value**
4B	VLT	3	F (3, 8) = 101.7	P < 0.0001	0.25 wt.% GO-QD	0.3284
					0.25 wt.% NGO-QD1	< 0.0001

					0.25 wt.% NGO-QD2	< 0.0001
	Blue- Light Blocking Ability	3	F (3, 8) = 473.8	P < 0.0001	0.25 wt.% GO-QD	0.0302
					0.25 wt.% NGO-QD1	< 0.0001
					0.25 wt.% NGO-QD2	< 0.0001
	UVA Blocking Ability	3	F (3, 8) = 275.7	P < 0.0001	0.25 wt.% GO-QD	0.002
					0.25 wt.% NGO-QD1	< 0.0001
					0.25 wt.% NGO-QD2	< 0.0001
	UVB Blocking Ability	3	F (3, 8) = 199.6	P < 0.0001	0.25 wt.% GO-QD	0.0005
					0.25 wt.% NGO-QD1	< 0.0001
					0.25 wt.% NGO-QD2	< 0.0001
	UVC Blocking Ability	3	F (3, 8) = 269.9	P < 0.0001	0.25 wt.% GO-QD	0.0001
					0.25 wt.% NGO-QD1	< 0.0001
					0.25 wt.% NGO-QD2	< 0.0001
7A	Tensile Strength	4	F (3, 20) = 5.422	P = 0.0068	0.25 wt.% GO-QD	0.2227
					0.25 wt.% NGO-QD1	0.0267
					0.25 wt.% NGO-QD2	0.0083
7B	Tensile Modulus	4	F (3, 12) = 6.507	P = 0.0073	0.25 wt.% GO-QD	0.0771
					0.25 wt.% NGO-QD1	0.0056
					0.25 wt.% NGO-QD2	0.0075
7C	Tensile Toughness	4	F (3, 12) = 24.16	P < 0.0001	0.25 wt.% GO-QD	0.1476
					0.25 wt.% NGO-QD1	0.0001
					0.25 wt.% NGO-QD2	< 0.0001
S1E	VLT	3	F (2, 6) = 131.5	P < 0.0001	0.1 wt.% NGO-QD2	0.0001
					0.25 wt.% NGO-QD2	< 0.0001
	Blue-Light Blocking Ability	3	F (2, 6) = 894.8	P < 0.0001	0.1 wt.% NGO-QD2	< 0.0001
					0.25 wt.% NGO-QD2	< 0.0001
	UVA Blocking	3	F (2, 6) =	P < 0.0001	0.1 wt.% NGO-QD2	< 0.0001

Ability		648.9			
				0.25 wt.% NGO-QD2	< 0.0001
UVB Blocking Ability	3	F (2, 6) = 743.2	P < 0.0001	0.1 wt.% NGO-QD2	< 0.0001
				0.25 wt.% NGO-QD2	< 0.0001
UVC Blocking Ability	3	F (2, 6) = 659.5	P < 0.0001	0.1 wt.% NGO-QD2	< 0.0001
				0.25 wt.% NGO-QD2	< 0.0001

References

1 J. D. Stachowska, A. Murphy, C. Mellor, D. Fernandes, E. N. Gibbons, M. J. Krysmann, A. Kelarakis, E. Burgaz, J. Moore and S. G. Yeates, *Sci. Rep.*, 2021, **11**, 1–14.

2 N. D. Sansone, Z. Razzaz, M. Salari, A. V. Tuccitto, R. Aguiar, M. Leroux and P. C. Lee, *ACS Appl. Mater. Interfaces*, 2022, **14**, 40232−40246.

3 A. V Tuccitto, A. Anstey, N. D. Sansone, C. B. Park and P. C. Lee, *Int. J. Biol. Macromol.*, 2022, **218**, 22–32.

4 E. W. Fischer, H. J. Sterzel and G. Wegner, *Kolloid-Zeitschrift Zeitschrift für Polym.*, 1973, **251**, 980–990.

5 R. Aguiar, O. E. Petel and R. E. Miller, *Compos. Part C Open Access*, 2022, **7**, 100231.

6 A. International Commission on Illumination (CIE), Vienna, CIE 2022, CIE standard illuminant D65, https://cie.co.at/datatable/cie-standard-illuminant-d65.

7 B. L. Diffey, *Methods*, 2002, **28**, 4–13.

8 J. H. Lee, S. H. Mahmood, J. M. Pin, R. Li, P. C. Lee and C. B. Park, *Int. J. Biol. Macromol.*, 2022, **204**, 274–283.